Spin confinement by anisotropy modulation

2002 J. Phys. D: Appl. Phys. 35 2384

(http://iopscience.iop.org/0022-3727/35/19/309)

INSTITUTE OF PHYSICS PUBLISHING JOURNAL OF PHYSICS D: APPLIED PHYSICS

J. Phys. D: Appl. Phys. **35** (2002) 2384–2390 PII: S0022-3727(02)35773-5

Spin confinement by anisotropy modulation

J A C Bland[1], W S Lew[1], S P Li[1], L Lopez-Diaz[1], C A F Vaz[1], M Natali[2] and Y Chen[2]

[1] Cavendish Laboratory, University of Cambridge, Madingley Road, Cambridge CB3 0HE, UK

[2] Laboratoire de Photonique et de Nanostructures, CNRS-LPN, Route de Nozay, Marcoussis 91460, France

E-mail: jacb1@phy.cam.ac.uk

Received 11 April 2001
Published 13 September 2002
Online at stacks.iop.org/JPhysD/35/2384

Abstract

The spin configuration in a magnet is in general a 'natural' consequence of both the intrinsic properties of the material and the sample dimensions. We demonstrate that this limitation can be overcome in a homogeneous ferromagnetic film by engineering an anisotropy contrast. Substrates with laterally modulated single-crystal and polycrystalline surface regions were used to induce selective epitaxial growth of a ferromagnetic Ni film. The resulting spatially varying magnetic anisotropy leads to regular perpendicular and in-plane magnetic domains, separated by a new type of magnetic domain wall–the 'anisotropy constrained' magnetic wall. Micromagnetic simulations indicate that the wall is asymmetric, has a small out-of-plane component and has no mobility under external perturbation.

1. Introduction

Controlling magnetic micro- and nano-structures and associated magnetization reversal processes are key issues for the future of magnetic information storage, and spin electronic devices [1–6]. Isolated 'island' magnetic structures such as dots [7–15], wires [16, 17], and other special geometries [18–21] have already been extensively studied. Such 'island' structures, supported on a substrate with no adjacent film in the vicinity, can be fabricated using a number of nano-fabrication techniques, including electron-beam lithography [7, 13, 18, 20, 22], x-ray lithography [23, 24], nanoimprint lithography [25, 26], and many others [27–29]. While the simplicity and establishment of the fabrication methods are advantages of these patterned structures, there are drawbacks such as poor planarity, abrupt change of optical index, and inconsistent magnetic switching behaviour due to irregular edges caused by the lithography process. The issue of medium planarity is particularly crucial for application purposes [30, 31].

A planar-patterned magnetic medium was first demonstrated by Chappert *et al* [32], where a He^+ ion irradiation technique was used to induce local chemical mixing in a Co/Pt multilayer film through a lithographically made polymer resist mask. The patterned magnetic structure obtained resulted from the modulated distribution of chemical components, without significantly modifying the topography. Using a different dose of ion energy, they can also effectively reduce the anisotropy, coercivity, and Curie temperature in the Co/Pt multilayer structures. It is suggested that the effect is likely due to local atomic relaxation and alloy formation [33–36]. More attempts include that of Terris *et al*, who have also used He^+ ion irradiation to locally modify the properties of a magnetic material through non-contact silicon stencil masks [37, 38]; that of Weller *et al*, who further found out that Co/Pt multilayer films undergo a spin orientation transition from out-of-plane to in-plane when irradiated with nitrogen ions [39]; and others [40].

The advance from 'island' to planar-patterned magnetic structures leads to the question: can we fabricate patterned structures in magnetic films which are not only continuous spatially, but also chemically homogeneous? The ultimate goal of such an approach is to control the local spin configurations in a given material. The spin configuration in a magnet is in general defined by both the intrinsic properties of the material and the sample dimensions. For instance, the domain pattern in a continuous Co film is determined either in random or in parallel stripe with the appropriate applied magnetic field [41, 42]; however, the spin configuration is

not locally controllable; Taniyama *et al* [43] have reported an artificially controllable 180° domain wall in sub-micron Co zigzag wires, and this artificially created domain wall, which was also observed by Xu *et al* [44] in a NiFe cross, was later analysed by Bruno as geometrically constrained walls [45]. However, the naturally formed domain structures do not have an exact reproducible switching mechanism and the geometrically constrained walls require, for instance, that the film must be sufficiently thick to have a significant shape anisotropy field. Overcoming this limitation so that the local spin configurations in continuous films can be systematically controlled can open up new avenues for fundamental studies and device applications. First, such structures can be used as a planar-patterned magnetic medium [32] without breaking the homogeneity of the magnetic film, which is important for avoiding reduced Curie temperature effects. More importantly, it introduces a new way to controlling spin configurations instead of stabilizing the natural domains [46]. Furthermore, such locally controlled spin configurations do not have lateral dimension limitations and thus can provide a reproducible switching mechanism, unlike the geometrically restricted domains [43, 44]. Such system is needed not only for ultrahigh-density magnetic storage and device applications, but also for fundamental studies. A film comprising regularly arranged regions with different magnetic anisotropy strengths for instance, constitutes a multi magnetic phase system which would allow the study of magnetic dipolar and exchange interactions, wall formation, and domain wall resistance in highly controlled geometries.

In this paper, a new type of magnetic medium [47, 48] is introduced where the spin configurations are engineered in chemically homogenous magnetic films using selective epitaxial growth[3]. Specifically, a regularly arranged in-plane and out-of-plane spin configuration defined by modulation of the magnetic anisotropy is demonstrated. Such a spin-engineered medium not only maintains the surface planarity but also the homogeneity of the magnetic materials, while the method holds advantages for immediate applications due to its simplicity and ease of integration.

2. Experiment

We demonstrate an approach of controlling the magnetic structure in chemically homogeneous films via the artificial modification of substrate surface properties prior to growth. A modulated single/polycrystalline substrate surface is used to locally modify the magnetic anisotropy in the subsequently deposited magnetic films, which induces the desired magnetic structure. Selective epitaxial growth introduces an alternation between single-crystal and polycrystalline structures in the film, according to the substrate patterning. We chose a well-studied epitaxial Cu/Ni/Cu(001) structure [49–55] to obtain an out-of-plane anisotropy. An epitaxial Ni(001) film with appropriate thickness shows perpendicular magnetic anisotropy (PMA) which is attributed to the magneto–elastic interaction induced by the Ni/Cu(001) interface [50]. In contrast, the magnetization of polycrystalline Ni lies in the film plane due to the dominant demagnetizing field. Figure 1 shows the schematic of the selective epitaxial growth. The substrates used are GaAs(001) and two types of pattern were chosen: a 2 μm width with 4 μm separation wire array, and a $7 \times 7\ \mu m^2$ area with 3 μm separation square dot array. Wire and dot arrays were obtained by optical lithography and a subsequent lift-off of 1 nm thick Ni. The ultrathin Ni patterns were then oxidized in air to become ultrathin NiO patterns. The patterned substrates were annealed at 500°C for 2 h before film growth at room temperature. Continuous films of Cu(5 nm)/Ni(5 nm)/Cu(70 nm)/Co(1.8 nm) were deposited onto the substrates in an ultrahigh vacuum system (10^{-10} mbar) using molecular beam epitaxy (MBE) techniques. The 1.8 nm thick Co is used as a seed layer to promote epitaxial growth on the GaAs substrate [56]. A thickness of 5 nm is selected for the Ni layer in order to obtain a strong PMA [49, 50, 53] and the 5 nm thick Cu overlayer is used to prevent oxidation. While the films grown on the ultrathin NiO patterns are polycrystalline, those grown directly onto the GaAs surface are single crystal films. The results have been confirmed by *in situ* reflection high-energy electron diffraction (RHEED) analysis. Figure 2 shows the obtained RHEED images with the electron beam (15 keV) parallel to the GaAs⟨100⟩ and GaAs⟨110⟩ axes. The diffraction circles and streaky-line/dot pattern reveals the co-existence of the polycrystalline and epitaxial regions in the substrates and films. Magneto-optical Kerr effect (MOKE) measurements were performed to obtain the hysteresis loops of the selective epitaxial samples. While magnetic force microscope (MFM) was used to study the magnetic domain structures, atomic force microscope (AFM) was used to examine the sample surface. Both MFM and AFM images were obtained simultaneously during the scanning.

3. Results and discussion

We carried out MOKE measurements at room temperature both in field-perpendicular-to-sample-film (polar) and field-parallel-to-sample-film (in-plane) geometries. The incidence angle of the laser in the polar and in-plane MOKE configurations was ∼0° and 35°, respectively. Spatially averaged MOKE signals are obtained from the patterned sample as the laser beam spot size was ∼1 mm. Figure 3 shows typical hysteresis loops measured from the samples. Loop (*a*) is a polar MOKE curve obtained from an unpatterned epitaxial reference sample. The perfectly square hysteresis behaviour with high remanence indicates a strong PMA in the epitaxial structure [51, 52]. The measured in-plane MOKE loop from the wire sample is shown in (*b*). The magnetic field was applied along the wire direction during the measurement and the hysteresis loop reveals the magnetization process in the sample. The switching at the field ∼100 Oe is due to the reversal of the in-plane magnetization in the polycrystalline regions. The sharp switch indicates that the reversal mechanism is controlled by domain nucleation and subsequent wall propagation. When the field is further increased towards saturation, the perpendicular magnetization in the epitaxial regions tends to align along the in-plane field direction through a magnetization rotation process, as evidenced by the high

[3] The term 'selective epitaxial growth' is also widely used in semiconductor technology. However, it refers to a process that allows the deposition of a Si epitaxial layer on a bare Si substrate surface without the simultaneous growth of amorphous Si thin film on the silicon dioxide surface, which is different from the process used in this work.

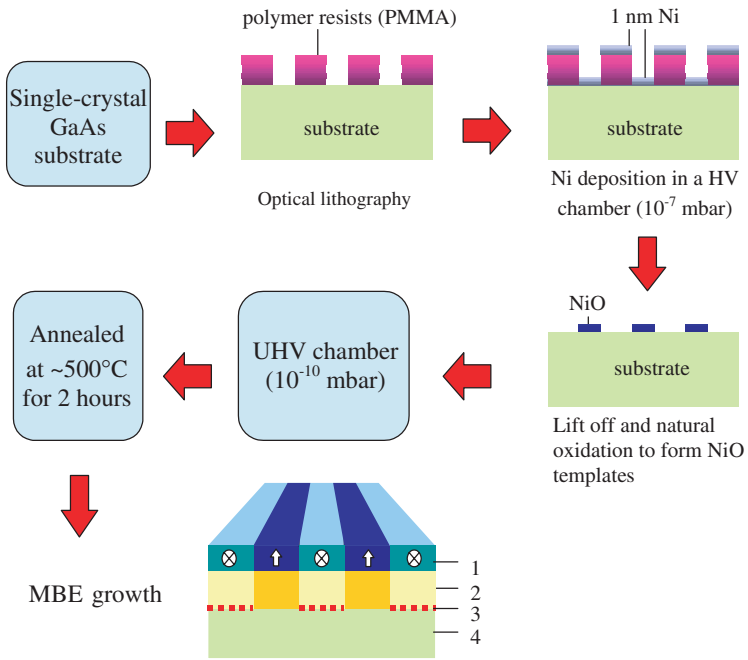

Figure 1. Schematic of the selective epitaxial growth of a Ni(001) film. 1: magnetic film (5 nm Ni); 2: underlayer (1.8 nm Co/70 nm Cu); 3: ultrathin template (1 nm NiO); 4: substrate (GaAs). The ultrathin NiO was used for the embedded pattern on a GaAs(001) substrate. The 1.8 nm thick Co was used as a seed layer to promote epitaxial growth on GaAs. The 70 nm thick Cu buffer layer is thick enough to prevent the Co seed layer signal from being detected in the MOKE measurements.

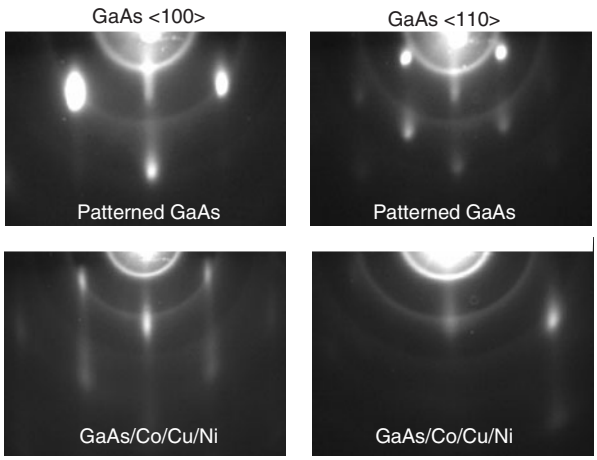

Figure 2. *In situ* RHEED images obtained from the selective epitaxial growth show the co-existence of the polycrystalline (diffraction circles) and epitaxial structure (diffraction dot/streaky-lines) in the patterned GaAs substrate and Ni films. Images at left and right column were taken with the electron beam parallel to the GaAs⟨100⟩ and GaAs⟨110⟩ axes, respectively.

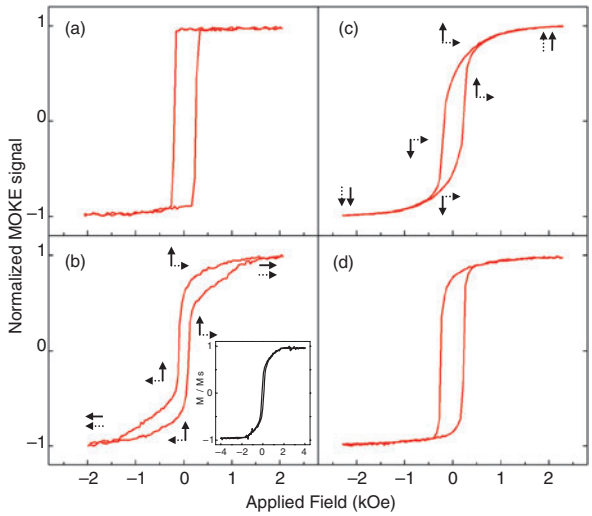

Figure 3. MOKE hysteresis loops at room temperature. (*a*) A polar MOKE loop measured on the epitaxial Ni from an unpatterned reference sample. (*b*) In-plane MOKE loop taken from the wire sample, inset shows the hysteresis loop measured by SQUID after subtracting the substrate signal. (*c*), (*d*) Polar MOKE loops measured on the wire and the dot samples, respectively. The solid (· · ·►) arrows show the magnetization orientations in the epitaxial (polycrystalline) Ni film. The magnetization orientations of the perpendicular Ni (up or down) in loop (*b*) and the in-plane Ni (right or left) in loop (*c*) is arbitrarily chosen.

saturation field. The irreversible behaviour near high field seen in the loop is due to the sensitivity of the in-plane MOKE geometry to the perpendicular component of the magnetization in epitaxial Ni [51]. A measurement that can respond only to the in-plane magnetization component can therefore be expected not to show such an irreversible feature, and this is confirmed by a superconducting quantum-interference device (SQUID) measurement (inset of loop (*b*)). Loops (*c*) and (*d*) show the measured polar MOKE results from the wire and dot samples, respectively. In this measurement geometry only the perpendicular magnetization component can be detected.

As the perpendicular field is reduced from positive saturation to zero, the magnetization in the polycrystalline Ni rotates back to the in-plane direction. However, the magnetization in the epitaxial Ni remains in the normal direction of the film. Upon increasing the field in the negative direction, the perpendicular magnetization switches to the reversed

direction at its coercive field (∼200 Oe), while the in-plane magnetization rotates progressively towards the out-of-plane direction in an increasing negative field. The polar MOKE loop obtained from the dot sample is squarer than that of the wire sample; this is because the area of the epitaxial Ni region in the dot sample is larger than that in the wire sample. The combined MOKE observations, supported by the sharp switch in low field and the gradual saturation seen in high field in both the in-plane and polar MOKE loops, clearly reveal the striking feature that *both* in-plane and out-of-plane magnetization co-exist in the patterned samples.

The magnetic structures deduced from MOKE magnetometry were confirmed by MFM imaging. In the MFM, the instrument was equipped with a CoCr coated Si tip, magnetized along the tip axis. During scanning, the magnetic tip oscillated at a chosen lift scan height while picking up the magnetic signal from the samples. Figures 4(*a*) and (*b*) show the MFM images of the dot and wire samples in the remanent state after saturating with a perpendicular field. A 100 nm lift scan height was used in these scans. The bright stripes in the images correspond to the out-of-plane Ni magnetization which has a strong magnetic signal and yields more contrast compared to the in-plane magnetization. To explore the reversal mechanism of the perpendicularly magnetized Ni, we carried out MFM observations under a lower lift scan height. Figures 4(*c*) and (*d*) show the MFM images scanned at a 50 nm lift scan height for the dot and wire samples, respectively, in the remanent state obtained after perpendicular saturation. The lower lift scan height enabled a stronger interaction between the emanating stray field from the tip and the samples. The dark regions in the out-of-plane Ni regions, encircled in white, are caused by the tip-induced switch. The high density of the reversed regions indicates a nucleation-dominated reversal process in our samples [57, 58]. The reversal stages, including domain nucleation, local expansion from the nuclei, and widening by domain wall displacement, are completed in a very small external field interval as indicated by the rapid switch in the MOKE loops. To verify this, we have repeated scanning in the centre with a smaller scan area until the magnetization there has been almost fully switched (see the $\sim 20 \times 20\ \mu m^2$ 'cut-off' at the centre of the images). The remaining unswitched hard magnetic entities near crystal defects, which define the final reversal stage, require higher magnetic fields to reverse. Figure 5 shows evolutions of the tip-induced switch in a scan area of $50 \times 50\ \mu m^2$ on the (*a*) dot sample and (*b*) wire sample. A close-up- scanned MFM image shows a strong dark contrast in the fully switched perpendicular Ni magnetization.

Roughness analyses were performed on the scanned AFM images using a software available to the commercial scanning probe microscope. The analyses yield two statistical roughness parameters: mean roughness R_a and root mean square roughness R_{rms}. The obtained R_a and R_{rms} values are 1.178 and 1.756 nm for the matrix sample and, 1.182 and 1.539 nm for the stripe sample, respectively. These values are comparable to the roughness data reported in literature in epitaxial Cu/Ni/Cu continuous films. Using polarized neutron reflectivity (PNR), Hope *et al* have obtained a range of interface roughness from 1.30 to 2.25 nm for different Ni thicknesses (3–40 nm) [54]. Therefore, the selective epitaxial sample produced in this work is considered a flat continuous Ni film. Figure 6 shows a typical profile analysis on a $50 \times 50\ \mu m^2$ matrix sample image.

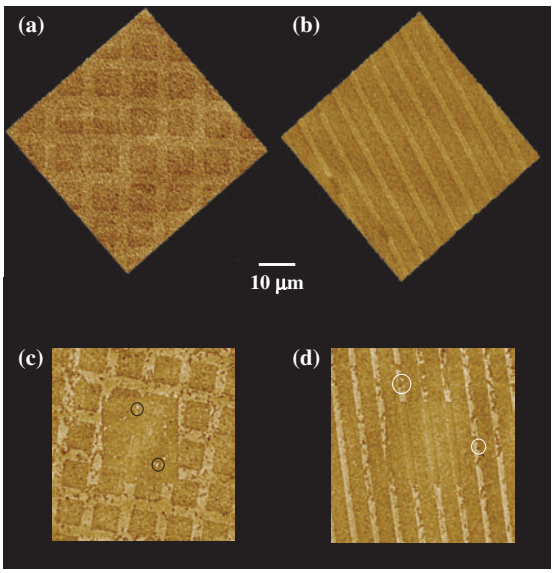

Figure 4. MFM images in zero applied field after perpendicular magnetic field saturation. 100 nm (*a*) and (*b*) and 50 nm (*c*) and (*d*) lift scan height were used. For 50 nm lift scan height, the magnetic stray field can induce switching in the perpendicularly magnetized Ni (the white circles mark the tip-induced switch in (*d*)). In the centre part of the image (*c*) and (*d*), the magnetization was almost fully switched by the repeated scans. The bright regions in the epitaxial Ni marked by black circles are the remaining unswitched hard magnetic entities after the repeated scans.

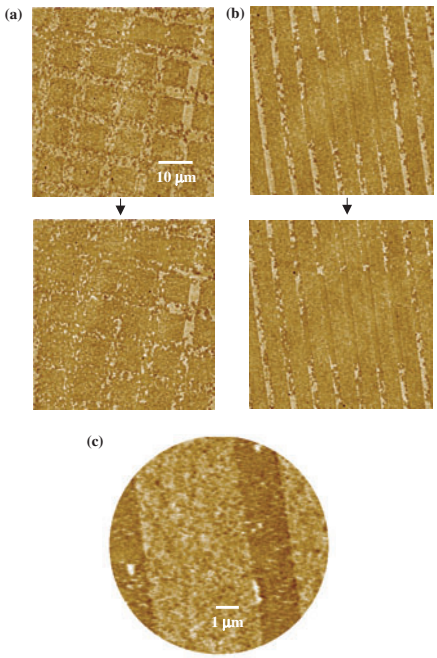

Figure 5. The perpendicular Ni magnetization is slowly switched by repeated scanning on the same $50 \times 50\ \mu m^2$ area with a lift height of 50 nm for (*a*) matrix sample, (*b*) stripe sample. Circle MFM image (*c*) is a close up for a repeated-scanned stripe sample with a lift height of 50 nm. The strong dark contrast in the epitaxial regions clearly shows the near fully switched magnetization. White dots in the epitaxial stripes are the above-mentioned hard magnetic entities.

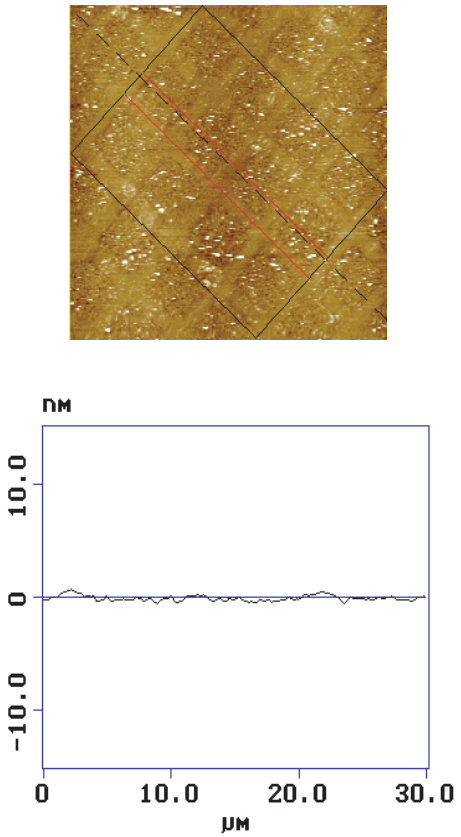

Figure 6. Profile analysis on a AFM image: a $30 \times 40\,\mu m^2$ averaged profile on a $50 \times 50\,\mu m^2$ dot sample image.

The 90° transition between the in-plane and out-of-plane regions is very sharp, as observed in figure 4. Figure 7 illustrates the spin orientation of the regions. To the author's knowledge, a domain wall of this kind has not been studied before. Consequently, micromagnetic numerical simulations were carried out in order to determine its width and internal structure. Using a conjugate gradient solver, the micromagnetic equilibrium equation was solved after saturating the sample along the perpendicular and in-plane directions. A cell size of 1 nm and typical Ni intrinsic parameters ($A = 9 \times 10^{-7}\,\mathrm{erg\,cm^{-1}}$, $M_s = 490\,\mathrm{emu\,cm^{-3}}$) were used in the simulation. $K_1 = 2.7 \times 10^6\,\mathrm{erg\,cm^{-3}}$ is the perpendicular anisotropy constant measured experimentally from Cu/Ni(5 nm)/Cu(001) films [55]. The magnetization configuration in the transition region is represented in figure 8(*a*). In figure 8(*b*), the variation of the out-of-plane component M_y along the z-direction is plotted, where $z = 0$ corresponds to the boundary between the epitaxial (left) and polycrystalline (right) regions. Actually, the obtained wall is different in detail from the well-known Bloch wall [59–61] and several new features can be observed. Firstly, it is an asymmetric wall due to the different anisotropy strength on both sides of the boundary. Secondly, the wall is constricted in the film with no mobility under external perturbation, which is particularly important for stable ultrahigh-density magnetic recording. Finally, it is important to note that immediately after the sharp transition there is a region with a small out-of-plane component ($M_y < 0$), which partially compensates the upwelling flux on the epitaxial region of the transition

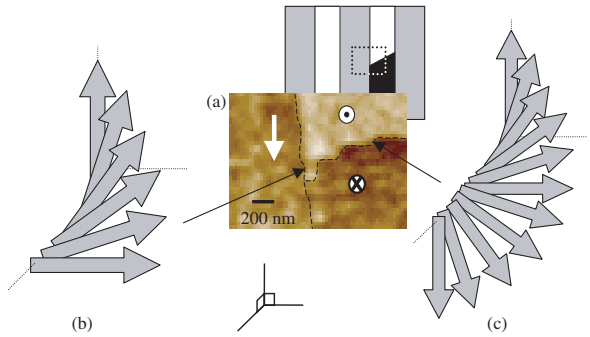

Figure 7. (*a*) A zero field MFM image (enlarged) of the Ni wire sample (cartoon) exhibiting (*b*) the new artificial 90° anisotropy constrained magnetic wall and (*c*) the well-known 180° Bloch wall which is defined by partial switch of the perpendicularly magnetized Ni inside the epitaxial wire structure. The white arrow indicates the in-plane magnetization, whereas the symbols ⊙ refer to the perpendicular upward magnetization, and ⊗ refers to the perpendicular downward magnetization.

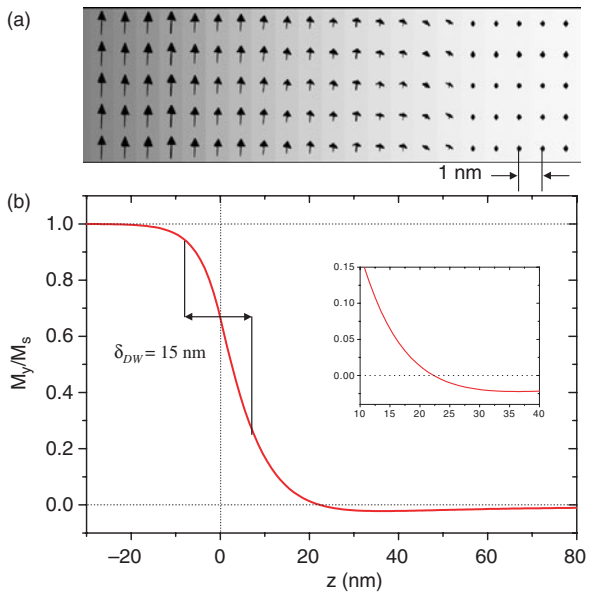

Figure 8. (*a*) Computed magnetization configuration of the transition between the epitaxial and polycrystalline regions. (*b*) Variation of the perpendicular component of the normalized magnetization across the boundary ($z = 0$) between the perpendicular and in-plane magnetized Ni. Note the asymmetry of the wall due to the different magnetic anisotropy strengths of the in-plane and perpendicular Ni. Inset (*b*) shows a close up of the small perpendicular component from the profile.

($M_y > 0$). A similar effect is found in vortex cores [60–62]. By looking at figure 8(*b*) the domain wall width is approximately 15 nm. The dependence of wall width (δ_{DW}) on the anisotropy constant K_1 and the film thickness t is weak. A factor of 2 in the value of K_1 yields a variation in δ_{DW} of less than 5%, whereas a change of 1 nm in t gives 1% variation in δ_{DW}. The domain wall width sets a fundamental limit for the high pattern density achievable using the method described in this report. Additional simulations have been carried out by taking into account the finite size of the structures: it is found that the well-defined out-of-plane to in-plane transitions can be obtained for structures with a resolution down to 30 nm (figure 9), which is quite promising for technological

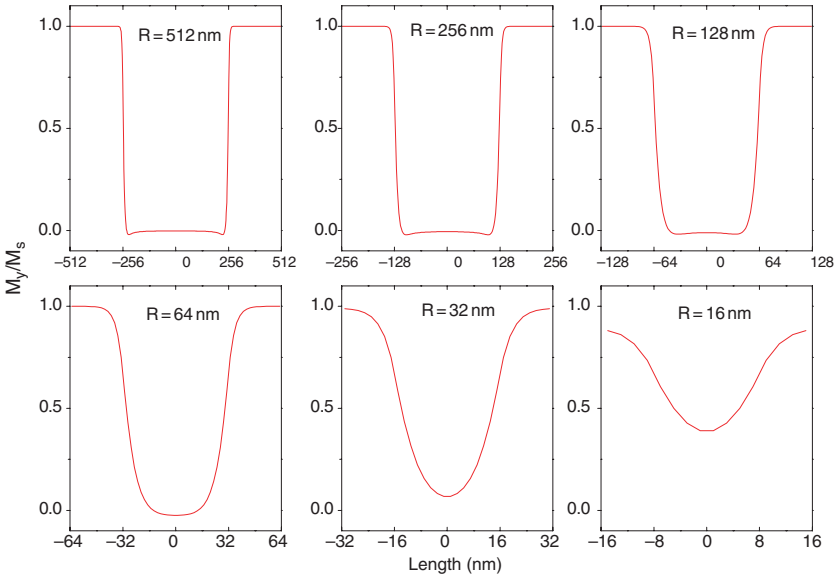

Figure 9. The magnetization profiles in different periodicity for the Ni wire structure. Resolution (R) is defined by a half period of the structure, where 0 is the centre of the polycrystalline Ni wire, and a period is taken as two times the width of the polycrystalline Ni wire.

applications. Mathematically, the wall length can also be expressed by the contributions of two Bloch walls:

$$\delta = \frac{\pi}{2}\left(\frac{1}{\sqrt{K_1 - 2\pi M_s^2}} + \frac{1}{\sqrt{2\pi M_s^2}}\right)\sqrt{A} \qquad (1)$$

Equation (1) yields $\delta \sim 15.5$ nm for the same parameters given above, which agrees well with the numerically simulated result.

4. Conclusion

In conclusion, we have created modulated magnetic structures in chemically homogeneous Ni films by inducing a spatially varying magnetic anisotropy via selective epitaxy. A new type of magnetic wall has been observed which we term the 'anisotropy constrained' magnetic wall. The wall structure differs from that of naturally occurring domain wall, e.g. the Néel and Bloch walls [59–63] or the geometrically restricted wall [43, 45]. The spin engineering of this magnetic medium, which can be seen as the integration of patterned features into continuous ferromagnetic films, opens up new avenues to control the spin structure of magnetic materials. Compared with existing planar media fabrication technique, this method has several advantages: lithography-induced defects associated with edges are minimized, inexpensive facilities are required and the approach complements present thin-film deposition techniques. Finally, our simulations also indicate that the patterned bit resolution can be defined at the deep submicron scale (∼30 nm) as is required for device applications and fundamental studies. Furthermore, the anisotropy constrained magnetic walls are static in nature, which provides a reproducible switching mechanism, contrary to that of the natural domain wall.

Acknowledgments

This research was supported by EC, ESPRIT program (MASSDOTS Project No 22464). WSL thanks the support of the Cambridge Commonwealth Trust. CAFV is supported by Programa PRAXIS XXI (Portugal).

References

[1] Prinz G A 1998 *Science* **282** 1660
[2] Prinz G A 1995 *Phys. Today* **48** 58
[3] Chou S Y 1997 *Proc. IEEE* **85** 652
[4] Ball P 2000 *Nature* **404** 918
[5] Johnson M 2000 *IEEE. Spectrum* **37** 33
[6] Wolf S A and Treger D 2000 *IEEE Trans. Magn.* **36** 2748
[7] Hehn M, Ounadjela K, Bucher J, Rousseaux F, Decanini D, Bartenlian B and Chappert C 1996 *Science* **272** 1782
[8] Gu E, Ahmad E, Gray S J, Daboo C, Bland J A C, Brown L M, Rührig M, McGibbon A J and Chapman J N 1997 *Phys. Rev. Lett.* **78** 1158
[9] Stamm C, Marty F, Vaterlaus A, Weich V, Egger S, Maier U, Ramsperger U, Fuhrmann H and Pescia D 1998 *Science* **282** 449
[10] Wernsdorfer W, Hasselbach K, Sulpice A, Benoit A, Wegrowe J-E, Thomas L, Barbara B and Mailly D 1996 *Phys. Rev.* B **53** 3341
[11] Fruchart O, Nozières J-P, Wernsdorfer W, Givord D, Rousseaux F and Decanini D 1999 *Phys. Rev. Lett.* **82** 1305
[12] Cowburn R P, Adeyeye A O and Welland M E 1998 *Phys. Rev. Lett.* **81** 5414
[13] Cowburn R P, Koltsov D K, Adeyeye A O, Welland M E and Tricker D M 1999 *Phys. Rev. Lett.* **83** 1042
[14] Raabe J, Pulwey R, Sattler R, Schweinböck T, Zweck J and Weiss D 2000 *J. Appl. Phys.* **88** 4437
[15] Pike C and Fernandez A 1999 *J. Appl. Phys.* **85** 6668
[16] Shearwood C, Blundell S J, Baird M J, Bland J A C, Gester M, Ahmed H and Hughes P H 1994 *J. Appl. Phys.* **75** 5249
[17] Adeyeye A O, Lauhoff G, Bland J A C, Daboo C, Hasko D G and Ahmed H 1997 *Appl. Phys. Lett.* **70** 1046
[18] Cowburn R P, Adeyeye A O and Welland M E 1999 *Europhys. Lett.* **48** 221
[19] Zhu J G, Zheng Y F and Prinz G A 2000 *J. Appl. Phys.* **87** 6668
[20] Li S P, Peyrade D, Natali M, Lebib A, Chen Y, Ebels U, Buda L and Ounadjela K 2001 *Phys. Rev. Lett.* **86** 1102
[21] Rothman J, Kläui M, Lopez-Diaz L, Vaz C A F, Bleloch A, Bland J A C, Cui Z and Speaks R 2001 *Phys. Rev. Lett.* **86** 1098

[22] New R M H, Pease R F W, White R L, Osgood R M and Babcock K 1996 *J. Appl. Phys*. **79** 5851
[23] Rousseaux F, Decanini D, Carcenac F, Cambril E, Ravet M F and Launois H 1995 *J. Vac. Sci. Technol.* B **13** 2787
[24] Wegrowe J E, Fruchart O, Nozieres J-P, Givord D, Rousseaux F, Decanini D and Amsermet J Ph 1999 *J. Appl. Phys*. **86** 1028
[25] Chou S Y, Krauss P R and Renstrom P J 1996 *Science* **272** 85
[26] Cui B, Wu W, Kong L, Sun X and Chou S Y 1999 *J. Appl. Phys*. **85** 5534
[27] Thurn-Albrecht T, Schotter J, Kastle G A, Emley N, Shibauchi T, Krusin-Elbaum L, Guarini K, Black C T, Tuominen M T and Russell T P 2000 *Science* **290** 2126
[28] Li S P, Lew W S, Xu Y B, Hirohata A, Samad A, Baker F and Bland J A C 2000 *Appl. Phys. Lett*. **76** 748
[29] Sun S, Murray C B, Weller D, Folks L and Moser A 2000 *Science* **287** 1989
[30] Ross C A, Smith H I, Savas T, Schattenburg M, Farhoud M, Hwang M, Walsh M, Abraham M C and Ram R J 1999 *J. Vac. Sci. Technol.* B **17** 3168
[31] Ross C A 2001 *Ann. Rev. Mat. Res*. **31** 203
[32] Chappert C, Bernas H, Ferré J, Kottler V, Jamet J P, Chen Y, Cambril E, Devolder T, Rousseaux F, Mathet V and Launois H 1998 *Science* **280** 1919
[33] Ferré J, Chappert C, Bernas H, Jamet J-P, Meyer P, Kaitasov O, Lemerle S, Mathet V, Rousseaux F and Launois H 1999 *J. Magn. Magn. Mater.* **198** 191
[34] Devolder T, Chappert C, Chen Y, Cambril E, Bernas H, Jamet J P and Ferré J 1999 *Appl. Phys. Lett*. **74** 3383
[35] Devolder T, Ferré J, Chappert C, Bernas H, Jamet J-P and Mathet V 2001 *Phys. Rev.* B **64** 064415
[36] Devolder T, Chappert C, Mathet V, Bernas H, Chen Y, Jamet J P and Ferré J 2000 *J. Appl. Phys*. **87** 8671
[37] Terris B D, Weller D, Folks L, Baglin J E E, Kellock A J, Rothuizen H and Vettiger P 2000 *J. Appl. Phys*. **87** 7004
[38] Terris B D, Folks L, Weller D, Baglin J E E, Kellock A J, Rothuizen H and Vettiger P 1999 *Appl. Phys. Lett*. **75** 403
[39] Weller D, Baglin J E E, Kellock A J, Hannibal K A, Toney M F, Kusinski G, Lang S, Folks L, Best M E and Terris B D 2000 *J. Appl. Phys*. **87** 5768
[40] Kaminsky W M, Jones G A C, Patel N K, Booij W E, Blamire M G, Gardiner S M, Xu Y B and Bland J A C 2001 *Appl. Phys. Lett*. **78** 1589
[41] Gregg J F, Allen W, Ounadjela K, Viret M, Hehn M, Thompson S M and Coey J M D 1996 *Phys. Rev. Lett.* **77** 1580
[42] Ruediger U, Yu J, Zhang S, Kent A D and Parkin S S P 1998 *Phys. Rev. Lett.* **80** 5639
[43] Taniyama T, Nakatani I, Namikawa T and Yamazaki Y 1999 *Phys. Rev. Lett*. **82** 2780
[44] Xu Y B, Vaz C A F, Hirohata A, Leung H T, Yao C C, Bland J A C, Cambril E, Rousseaux F and Launois H 2000 *Phys. Rev.* B **61** R14901
[45] Bruno P 1999 *Phys. Rev. Lett*. **83** 2425
[46] Krusin-Elbaum L, Shibauchi T, Argyle B, Gignac L and Weller D 2001 *Nature* **410** 444
[47] Li S P, Lew W S, Bland J A C, Lopez-Diaz L, Natali M, Vaz C A F and Chen Y 2002 *Nature* **415** 600
[48] Li S P, Lew W S, Bland J A C, Lopez-Diaz L, Vaz C A F, Natali M and Chen Y 2002 *Phys. Rev. Lett*. **88** 087202
[49] O'Brien W L and Tonner B P 1994 *Phys. Rev.* B **49** 15370
[50] Jungblut R, Johnson M T, aan de Stegge J, Reinders A and den Broeder F J A 1994 *J. Appl. Phys*. **75** 6424
[51] Lee J, Lauhoff G and Bland J A C 1997 *Phys. Rev.* B **56** R5728
[52] Vaz C A F and Bland J A C 2000 *Phys. Rev.* B **61** 3098
[53] Bochi G, Ballentine C A, Inglefield H E, Thompson C V, O'Handley R C, Hug H J, Stiefel B, Moser A and Güntherodt H-J 1995 *Phys. Rev.* B **52** 7311
[54] Hope S, Lee J, Rosenbusch P, Lauhoff G, Bland J A C, Ercole A, Bucknall D, Penfold J, Lauter H J, Lauter V and Cubitt R 1997 *Phys. Rev.* B **55** 11422
[55] Bochi G, Ballentine C A, Inglefield H E, Thompson C V and O'Handley R C 1996 *Phys. Rev.* B **53** R1729
[56] Lew W S, Samad A, Li S P, Lopez-Diaz L, Cheng G X and Bland J A C 2000 *J. Appl. Phys.* **87** 5947
[57] Pommier J, Meyer P, Pénissard G, Freeé J, Bruno P and Renard D 1990 *Phys. Rev. Lett.* **65** 2054
[58] Bochi G, Hug H J, Paul D I, Stiefel B, Moser A, Parashikov I, Güntherodt H-J and O'Handley R C 1995 *Phys. Rev. Lett*. **75** 1839
[59] Bloch F 1932 *Z. Phys.* **74** 295
[60] Hubert A and Schäfer R 1998 *Magnetic Domains: The Analysis of Magnetic Microstructures* (Berlin: Springer)
[61] Landau L D and Lifshitz E M 1935 *Phys. Z. Sowjetunion* **8** 153
[62] Shinjo T, Okuno T, Hassdorf R, Shigeto K and Ono T 2000 *Science* **289** 930
[63] Néel L 1955 *C. R. Acad. Sci., Paris* **241** 533